International Journal of Advanced Engineering and Technology Research
ISSN: 3106-8677 (Print), ISSN: 3106-8685 (Online) | Vol. 3, No. 3, 2026

Time-Efficient Active Bearing-Only Localization with Reception and Coverage Guarantees

Ao Xiao *, Fangfang Zhou, Qiteng Guo

College of Mathematics and Statistics, Northwest Normal University, Lanzhou, 730070, China

* **Corresponding author**: (Email: xiaoao2math@163.com)

Abstract: Observation locations in bearing-only localization affect travel, uncertainty, and subsequent measurement requirements. We study a mobile sensor locating and removing a stationary omnidirectional radio source with bounded bearing errors and an unknown reception radius within known bounds. After initial detection, the second observation point minimizes expected remaining action time under a fixed continuation policy, subject to reliable reception and eventual completion. A th ree-disk intersection screens reception-safe candidates. The minimum enclosing circle of the bearing-consistent region certifies whether a removal disk covers every possible source location. Monte Carlo simulations evaluate complete missions, including travel, readings, and removal; a finite fallback scan guarantees completion under the model assumptions. In the reference case, 5,000 independent validation missions average 60.40 s, reducing time by 19.39% against a prescribed lateral point and 0.79% against a short-travel point. All 25,000 validation missions across five initial geometries succeed. An objective ablation shows that minimizing travel or reading count alone can increase completion time. The contribution is the integration of reception constraints, geometric coverage, and complete-mission time evaluation for reliable, time-efficient observation selection.

Keywords: Bearing-only localization, active sensing, reception guarantee, geometric coverage, expected completion time.

1. Introduction

A single bearing leaves the distance to a radio source uncertain. Moving a sensor laterally improves triangulation, but the move consumes time and may take the sensor beyond its reception range. Moreover, a position that supports accurate estimation need not permit the terminal operation: all source locations consistent with the observations must fit inside its coverage disk. Observation selection therefore links sensing geometry to physical mission completion. The relevant cost includes the next move, any further readings, travel to the terminal point, and removal. A short initial move or a small measurement count alone does not capture that cost.

Active bearing-based localization has been studied using geometric guarantees and statistical estimation. For bounded angular errors, Tokekar and Isler derived worst-case area and diameter bounds from wedge intersections [1]. More recently, Pozzan et al. combined weighted least squares with covariance-driven active sensing under Gaussian noise [2]. Peng et al. optimized UAV trajectories to enhance observability while estimating bearing-sensor bias [3]. In a multi-sensor setting, Jiang et al. balanced tracking performance and network energy through information-based sensor selection and dynamic clustering [4]. These objectives address localization quality or sensing resources, but they do not directly provide the terminal coverage test used here. We ask whether a reliably received sequence of observations permits a removal disk to cover every source location consistent with the measurements, and how long the full sequence takes.

The distinction matters when reception radius is uncertain. An attractive geometric baseline may be unreachable without losing the signal, and a small feasible-region diameter does not by itself certify coverage by a disk of prescribed radius. Li and Nie used an area of uncertainty to express directional position errors in underwater bearing-only tracking [5]. Here, we retain all positions consistent with bounded bearing errors, rather than substitute a point estimate for a completion certificate. Geometric guarantees depend on the error bound and physical assumptions, whereas expected-time comparisons depend on a specified source and error distribution. Keeping these roles separate allows simulated efficiency gains to be interpreted without treating successful trials as a proof of universal reliability.

We use the setting of Problem B in the 2026 Contemporary Undergraduate Mathematical Contest in Modeling [6], focusing on one stationary omnidirectional source after its first normal detection. A related preprint describes whole-region search and completion certification for multiple emitters with unknown directionality [7]; its broader task differs from the second-observation decision studied here. We select that observation under an unknown source location, an unknown bounded reception radius, and bounded bearing error. First, a three-disk safe region screens candidates. Wedge intersections and their minimum enclosing circle determine whether to remove the source or continue sensing. With continuation fixed, Monte Carlo simulation ranks candidates by full remaining action time, and finite fallback guarantees completion under the model assumptions. We validate the selected points in five initial geometries and examine cost sensitivity and objective ablations. Optimization is restricted to a finite candidate set and one decision stage; the results do not establish a globally optimal sensing policy.

2. Geometric Constraints

2.1. Sensing and Terminal Coverage

Let the stationary source be $G \in D=B(0,a) \subset R^2$, where $B(C,r)$ is a closed disk. Positions A_i are known accurately, and motion is unobstructed at speed $v_m>0$. A fixed unknown reception radius satisfies $R_{min} \le R \le R_{max}$. A normal reading is available at distance $r_{near}<\|G-A_i\| \le R$; a close-range flag at distance at most $r_{near} \le \rho$ permits removal at the current

position. Otherwise the sensor receives no signal. Normal readings satisfy

$$\theta_i=\operatorname{atan2}(G_y-A_{iy},G_x-A_{ix})+\epsilon_i,\quad |\epsilon_i|\le\alpha,\quad 0<\alpha<\pi/2 \tag{1}$$

Angles are modulo 2π. Set $e_i=(\cos\theta_i,\sin\theta_i)^T$, $n_i=(-\sin\theta_i,\cos\theta_i)^T$, $s_i(P)=(P-A_i)^T e_i$, and $t_i(P)=(P-A_i)^T n_i$. The bearing-consistent wedge and its intersection are

$$W_i=\{P: s_i(P)\ge 0,\ |t_i(P)|\le s_i(P)\tan\alpha\},\qquad \Omega_n=\bigcap_{i\in I_n} W_i \tag{2}$$

Here I_n indexes retained normal readings among the first n attempts. Enumerating feasible intersections of nonparallel boundaries, removing duplicates, and checking unbounded directions gives the vertices V_n when Ω_n is bounded. Convexity gives $\Omega_n=\operatorname{conv}(V_n)$ and $D_n=\max_{p,q\in V_n}\|p-q\|$. The minimum enclosing circle [8] is determined by at most three vertices:

$$r_n=\min_C \max_{P\in\Omega_n}\|P-C\|,\quad C_n\in\operatorname*{argmin}_C \max_{P\in\Omega_n}\|P-C\| \tag{3}$$

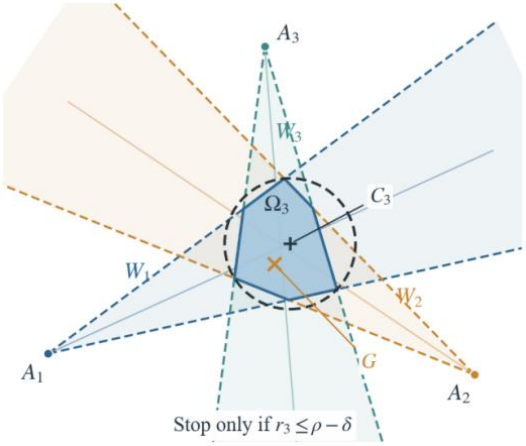


Figure 1. Bearing wedges and the minimum enclosing circle for terminal coverage

We test pair-diameter circles and noncollinear triple circumcircles; a singleton has radius zero and an unbounded region has infinite radius. Stop normal sensing when $r_n\le\rho-\delta$ and move to C_n. Since $G\in\Omega_n$, $\|G-C_n\|\le r_n<\rho$ certifies removal. We use $\delta=0.01$ m and inflate computed radii for tolerance. The diameter condition $D_n\le 2\rho$ is insufficient: an acute triangle with longest side D and opposite angle $\gamma<\pi/2$ has enclosing radius $D/(2\sin\gamma)>D/2$. At $D=2\rho$, it passes the diameter test but cannot be covered. Figure 1 illustrates the wedge and circle construction.

2.2. Reception-safe Second Observations

The first normal reading gives $F_1=D\cap W_1\cap\{G: r_{near}<\|G-A_1\|\le R_{max}\}$. For each compatible source, the smallest compatible radius is $\max\{R_{min},\|G-A_1\|\}$.

Thus the exact region guaranteeing a normal reading or close-range flag is

$$C_{recv}=\bigcap_{G\in F_1} B(G,\max\{R_{min},\|G-A_1\|\}) \tag{4}$$

Enlarge F_1 to the complete sector $\tilde{F}_1=\{A_1+re(\theta_1+\omega): 0\le r\le R_{max},\ |\omega|\le\alpha\}$, where $e(\theta)=(\cos\theta,\sin\theta)^T$. Its exact reception region is the conservative filter

$$C_{safe}=B(A_1,R_{min})\cap B(A_1+R_{min}e(\theta_1-\alpha),R_{min})\cap B(A_1+R_{min}e(\theta_1+\alpha),R_{min})\subseteq C_{recv}. \tag{5}$$

To prove the reduction, write $q=A_1+ue_1+vn_1$ and $h_\omega=u\cos\omega+v\sin\omega$. Then $\|q-G\|^2=r^2+u^2+v^2-2rh_\omega$. For $0\le r\le R_{min}$, convexity in r reduces reception to the endpoints: $u^2+v^2\le R_{min}^2$ and $u^2+v^2\le 2R_{min}h_\omega$. For larger r, the latter condition ensures $h_\omega\ge 0$, so $u^2+v^2\le 2rh_\omega$ cannot tighten. The angular endpoint conditions imply $u\ge 0$, hence $\min_{|\omega|\le\alpha}h_\omega=u\cos\alpha-|v|\sin\alpha$. Checking the apex and the two angular endpoints at R_{min} is therefore necessary and sufficient. The implementation tests

$$u^2+v^2\le R_{min}^2,\qquad u^2+v^2\le 2R_{min}(u\cos\alpha-|v|\sin\alpha) \tag{6}$$

The filter is exact for the enlarged sector, conservative for F_1, and independent of R_{max} once $R_{max}\ge R_{min}$. Figure 2 shows the disk intersection.

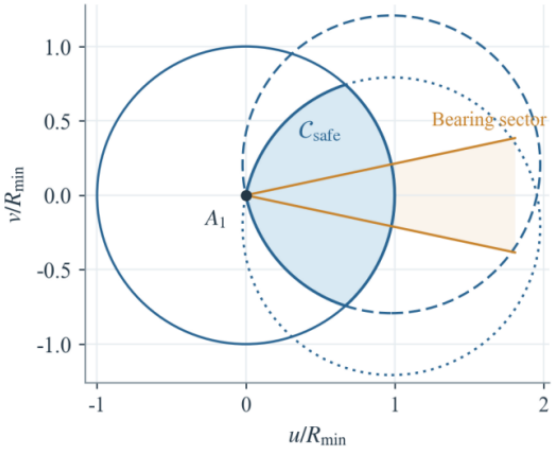


Figure 2. Reception-safe region defined by the three-disk intersection

3. Expected Mission Time and Completion

3.1. Objective and Monte Carlo Selection

Time starts after the first reading. If K is the final reading attempt and C_K the terminal point, all moves and reading attempts, including silent fallback attempts, contribute:

$$L_\pi=\sum_{i=1}^{K-1}\|A_{i+1}-A_i\|+\|C_K-A_K\|,\quad T_\pi=L_\pi/v_m+\tau_m(K-1)+\tau_t \tag{7}$$

Computation time is excluded. For close-range completion, $C_K=A_K$. We specify an area-uniform source distribution on F_1, not an inferred posterior: sample uniform angle and uniform squared radius, rejecting sources outside D. Future errors at distinct positions are independent uniform variables on $[-\alpha,\alpha]$; revisits reuse the original reading. Guarantees use only bounds, not these distributions. No distribution for R is needed because normal sensing guarantees reception and fallback uses only close-range feedback.

Let Ξ contain all compatible sources, radii, and bounded error sequences, and let $S_\pi(q;\xi)=1$ denote finite, successful completion. For fixed continuation π, success is a hard constraint:

$$\min_{q\in C_{safe}} f_\pi(q),\quad f_\pi(q)=E[T_\pi(q;\xi)],\quad S_\pi(q;\xi)=1 \text{ for every } \xi\in\Xi \tag{8}$$

At q, close-range feedback permits removal; otherwise a normal bearing updates Ω_n. If its enclosing circle fits the removal disk, the sensor moves to its center for service. Otherwise it continues sensing; exhaustion of admissible points or the reading limit triggers fallback. Monte Carlo

evaluation [9] averages the times of these complete missions, including every branch. The sample-average approximation [10] is

$$\hat{f}_M(q)=\frac{1}{M}\sum_{j=1}^{M} T_\pi\,(q;G^{(j)},\epsilon^{(j)}) \tag{9}$$

Candidates share random draws for paired comparisons, following the common-random-number approach used in simulation optimization [11]. A 20 m grid over $0\le u\le 1000$, $-880\le v\le 880$ passes the filter (6); a 2 m grid refines ±20 m around the best point and its reflection. The reference has 3021 coarse points and 3885 distinct points overall. The selected point minimizes the sampled mean on this finite set. Independent validation reports $\bar{T}\pm 1.96 s_T/\sqrt{N}$; paired intervals use within-mission differences. These approximate 95% intervals measure sampling error, not model uncertainty.

3.2. Fixed Continuation and Finite Fallback

Maintain Ω_n and a bounded planning polygon $\hat{\mathrm{F}}_n$ containing the source. Initialize the latter by intersecting bearing half-planes with outer tangent approximations of D and the first reception disk (normals every 0.25°); relax close-range exclusion to $s_1\ge r_{\text{near}}\cos\alpha$. New wedges clip the polygon, while the stopping certificate uses Ω_n.

From its enclosing-circle center $\hat{C}_n$, generate unvisited points $q=\hat{C}_n\pm bn_1$, $b\in\{40,80,160\}$ m. Accept a point if it belongs to a safe region from any previous normal reading or all planning vertices lie within $R_{\min}$ of it. Convexity extends the latter test to the polygon. For ranking, use three representative sources: $\hat{C}_n$ and its midpoints with the minimum- and maximum-u vertices. Append their noiseless bearings and let $\tilde{r}(q)$ be the largest resulting enclosing radius. With $\ell(q)=(\|A_n-q\|+\|q-\hat{C}_n\|)/v_{\text{m}}$, choose the lowest score

$$J(q)=\begin{cases}\ell(q), & \tilde{r}(q)\le\rho-\delta,\\ 10^6+\tilde{r}(q)+10^{-4}\ell(q), & \text{otherwise.}\end{cases} \tag{10}$$

The score uses meters and seconds and only guides selection; real bearings determine coverage. After eight readings beyond the first, or if no candidate remains, scan a 3 m square lattice over the planning rectangle in serpentine order. Round bounds outward and pad by one spacing. The scan ignores all feedback except the close-range flag and retains every attempt's cost.

Completion guarantee. Assume exact geometry, accurate unobstructed motion, bounded bearing errors, reliable feedback and service, and $0<r_{\text{near}}\le\rho$. If lattice spacing h satisfies $h\sqrt{2}/2\le r_{\text{near}}$, every compatible mission completes. Indeed, each wedge and outer planning approximation contains the true source. Normal stopping succeeds by (3), and close-range stopping by $r_{\text{near}}\le\rho$. Otherwise, normal sensing ends after finitely many attempts. The bounded, padded rectangle contains a nearest lattice point within $h\sqrt{2}/2$ of the source. A finite scan reaches it and triggers successful service. Thus geometry establishes completion; simulations estimate its cost. We distinguish final success from $p_2=\Pr(K=2)$, completion without a third reading.

4. Numerical Study

4.1. Parameters and Reference Case

Table 1 gives the parameters. Reference C2 uses $A_1=(1500,0)$ m and $\theta_1=0.4°$. Training and independent validation each use 5000 missions, with seeds 20260912 and 20260913. These are conditional single-source simulations, not official multi-source tests. The reproducibility package supplies code, samples, and candidate values; checks verify time accounting, 2000 random reception-filter tests, and the acute-triangle counterexample. The reception proof, rather than sampled checks, establishes safety.

Table 1. Simulation and search parameters

Parameter	Value	Parameter	Value
a	1800 m	r_{near}	5 m
$R_{\min}$	1000 m	ρ	20 m
$R_{\max}$	1500 m	δ	0.01 m
α	1°	v_{m}	5 m/s
τ_m	5 s	τ_t	5 s
Training M	5000	Validation N	5000
Coarse grid	20 m	Fine grid	2 m

Selection gives local coordinates (106,-34) m, global $A_2^*=(1606.235,-33.259)$ m, and initial travel 111.32 m. Training and validation means are 60.16 and 60.40 s; validation has standard error 0.223 s and a 95% interval [59.96,60.84] s. Figure 3 shows the sampled objective, and Figure 4 illustrates the two completion branches. Every validation mission succeeds without fallback; maximum terminal distance is 17.78 m, below $\rho=20$ m. Of the missions, 52.16% need no third reading and 47.84% need one more. Mean time comprises 48.007 s travel, 7.392 s readings, and 5 s service. The policy uses observed feedback; true sources generate feedback and verify terminal distances.

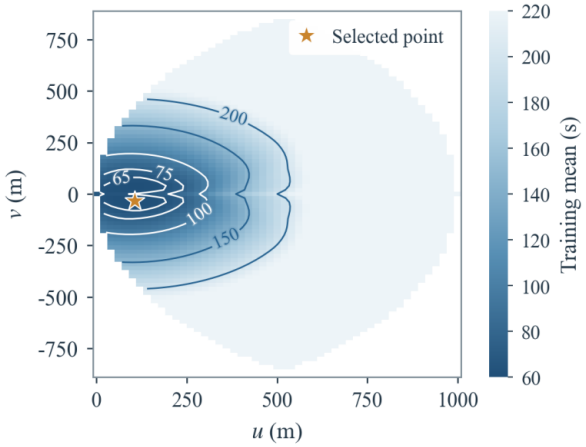


Figure 3. Sampled expected mission time over second-observation candidates

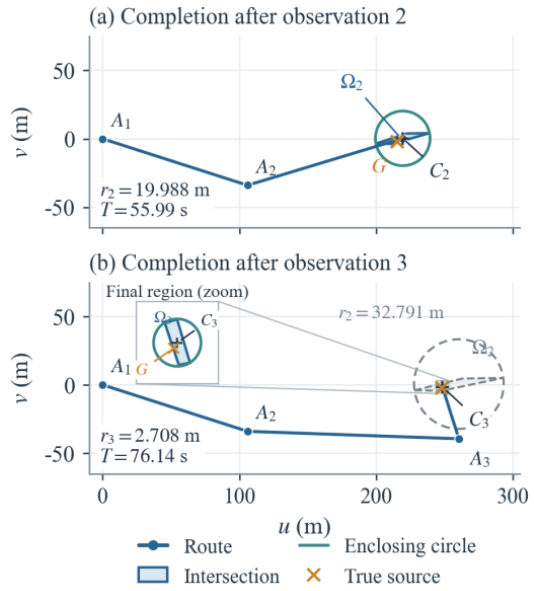


Figure 4. Direct and continued completion paths with their feasible regions

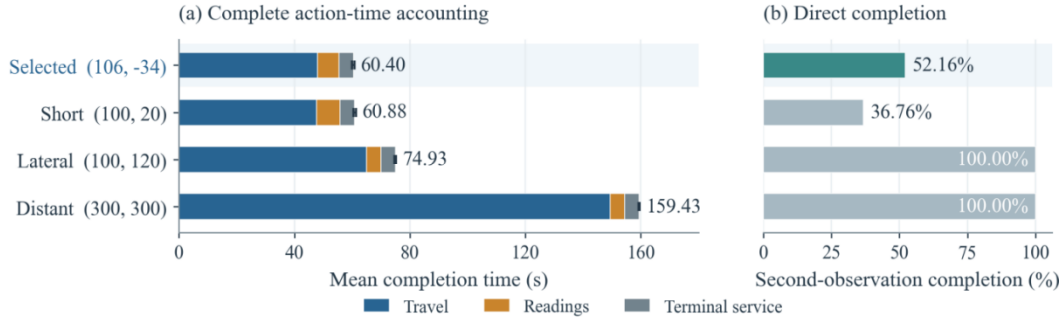


Figure 5. Time accounting and completion branches for the reference designs

Holding trajectories and decisions fixed, the short-minus-selected sample-mean difference is

$$\overline{\Delta T} = -1.4589/v_m + 0.1540\,\tau_m \qquad (11)$$

Figure 6 covers $2.5 \le v_m \le 10$ m/s and $0.5 \le \tau_m \le 10$ s. The selected point has lower sampled mean above $v_m \tau_m = 9.473$ m. At $(v_m, \tau_m) = (5,1)$, the difference is -0.138 s, favoring short travel, but its interval [-0.292,0.017] s includes zero. This is fixed-trajectory cost recalculation, not reoptimization or a noise-robustness test.

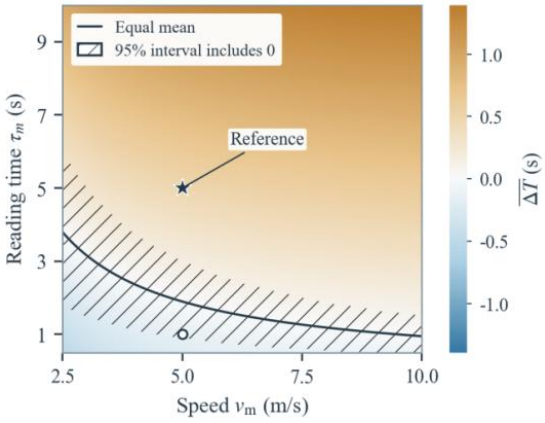


Figure 6. Fixed-trajectory sensitivity to motion speed and reading time.

4.3. Initial Geometries and Objective Ablation

We repeat selection in five geometries with unchanged parameters, grids, and continuation (Table 2). Each has 5000 training and 5000 independent validation missions. Feasible along-bearing source distances extend approximately to 100, 300, 800, 995, and 1500 m in C1–C5. All 25,000 selected-point validation missions succeed without fallback; maximum terminal distance is 19.20 m. Some C3–C5 missions need a fourth reading. The paired gains against fixed short and lateral designs have positive intervals (Figure 7); lateral-point gains range from 9.08 to 41.18 s. In C5, 36,442 of 19,425,000 training candidate–mission evaluations use fallback with full costs, which is not the selected policy's fallback probability.

4.2. Baselines and Sensitivity

Under identical continuation rules, prescribed lateral (100,120) m, short-travel (100,20) m, and distant (300,300) m points average 74.93, 60.88, and 159.43 s, respectively. These are fixed designs, not reproduced published algorithms. All complete every validation mission. Selection saves 14.53 s against the lateral point (19.39%; paired interval [14.28,14.78] s) and 0.478 s against the short point (0.79%; [0.289,0.668] s). Against the short point, it adds 0.292 s travel but saves 0.770 s reading time; direct completion rises from 36.76% to 52.16% (Figure 5).

Table 2. Independent validation in five initial geometries

Case	r (m)	θ_1 (°)	(u*, v*) (m)	Mean T (s)	p_2 (%)
C1	1700	0	(34, 12)	25.33	98.40
C2	1500	0.4	(106, −34)	60.40	52.16
C3	1000	0	(212, 54)	133.74	18.90
C4	1500	90	(292, 74)	162.85	18.20
C5	1500	180	(436, −116)	245.27	13.38

$A_1 = (r, 0)$; θ_1 is measured from global +X. Selected points use first-bearing coordinates. Each case has 5000 validation missions; p_2 is direct completion, not final success.

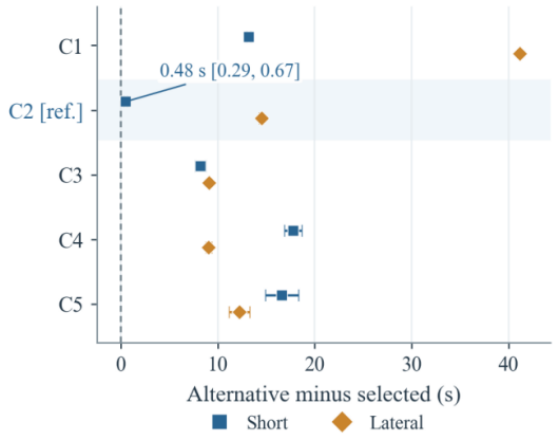


Figure 7. Paired time gains across five initial geometries

Independent 100,000-mission checks in C2 and C5 give short-minus-selected differences of 0.502 s [0.459,0.544] and 16.295 s [15.920,16.670]. Both policies complete every mission without fallback (400,000 executions total). No observed fallback implies neither zero probability nor validation of every model assumption. Full offline search and validation take 79–186 s per geometry with eight CPU threads; these costs are excluded from (7).

The ablation compares time, travel, and reading-count objectives on the same 3021 coarse points, 5000 training missions, and 5000 held-out missions per case, without refinement. Reading-count ties use less travel; travel ties use fewer readings; remaining ties use lexicographic coordinates. Table 3 reports mean time. Time and travel select the same point in C1, C3, and C4. Travel-only selection adds 0.348 s [0.141,0.554] in C2 and 0.319 s [0.102,0.535] in C5. Reading-only selection raises time in C2–C5, despite fewer readings. All choices complete all missions. The ablation isolates the objective, without claiming superiority to published methods.

Table 3. Mean action time (s) for the coarse-grid objective ablation

Case	Time objective	Travel objective	Reading objective
C1	26.40	26.40	26.40
C2	60.55	60.90	66.33
C3	133.78	133.78	281.45
C4	162.92	162.92	285.90
C5	245.32	245.63	310.92

5. Conclusions

This study establishes an implementable framework for selecting a second observation in active bearing-only localization while preserving reception and terminal coverage guarantees. The three-disk filter provides an explicit reception-safe candidate region, the minimum enclosing circle certifies removal coverage, and the finite fallback scan ensures completion under the stated assumptions. These geometric tests connect observation selection to a verifiable physical outcome. Complete-mission Monte Carlo evaluation then accounts for travel, additional readings, and service within a single decision criterion.

Across five initial geometries, all 25,000 selected-point validation missions completed successfully. In the reference case, the mean action time was 60.40 s, improving on the prescribed lateral and short-travel designs by 19.39% and 0.79%, respectively. Together with the objective ablation and cost sensitivity results, these findings support the feasibility of balancing motion and sensing costs through the proposed framework. Its guarantees remain conditional on bounded errors and idealized motion and reception, and computation is excluded from the reported action time. Future work will jointly optimize observation selection and continuation, develop faster online evaluation, and compare the framework with published active-localization methods. Further studies should incorporate navigation uncertainty, obstacles, multipath outliers, and alternative source distributions, followed by field experiments to assess practical performance.

References

[1] Tokekar, P., & Isler, V. (2013). Sensor placement and selection for bearing sensors with bounded uncertainty. In 2013 IEEE International Conference on Robotics and Automation (pp. 2515–2520). IEEE.

[2] Pozzan, B., Michieletto, G., Mesbahi, M., & et al. (2024). An active-sensing approach for bearing-based target localization. In 2024 American Control Conference (pp. 2752–2757). IEEE.

[3] Peng, J., Wang, Q., Jin, B., & et al. (2024). Trajectory optimization to enhance observability for bearing-only target localization and sensor bias calibration. Biomimetics, 9(9), 510.

[4] Jiang, X., Ma, T., Jin, J., & et al. (2023). Sensor management with dynamic clustering for bearings-only multi-target tracking via swarm intelligence optimization. Electronics, 12(16), 3397.

[5] Li, H., & Nie, Z. (2024). Underwater bearing-only passive target tracking method based on area of uncertainty. Journal of Electronics & Information Technology, 46(1), 109–117. (In Chinese).

[6] Cumcm Organizing Committee. (2026, September 10). Problem B: Rapid automatic localization and removal of radio interference sources [EB/OL]. Retrieved October 9, 2026.

[7] Cao, C., & Ouyang, Z. (2026, September 13). Certifiable search and neutralization of radio emitters with unknown directionality using a bearing-only mobile sensor [Preprint]. SSRN. Retrieved October 9, 2026.

[8] Welzl, E. (1991). Smallest enclosing disks (balls and ellipsoids). In H. Maurer (Ed.), New Results and New Trends in Computer Science (pp. 359–370). Springer.

[9] Hung, Y. C. (2024). A review of Monte Carlo and quasi-Monte Carlo sampling techniques. WIREs Computational Statistics, 16(1), e1637.

[10] Peng, Y., Chen, C. H., & Fu, M. C. (2026). A review of simulation optimization with connection to artificial intelligence. Fundamental Research, 6(3), 1848–1858.

[11] Eckman, D. J., Henderson, S. G., & Shashaani, S. (2023). SimOpt: A testbed for simulation-optimization experiments. INFORMS Journal on Computing, 35(2), 495–508.